Article

Charge Transport in Single Au | Alkanedithiol | Au Junctions: Coordination Geometries and Conformational Degrees of Freedom

Chen Li, Ilya Pobelov, Thomas Wandlowski, Alexei Bagrets, Andreas Arnold, and Ferdinand Evers

J. Am. Chem. Soc., **2008**, 130 (1), 318-326 • DOI: 10.1021/ja0762386

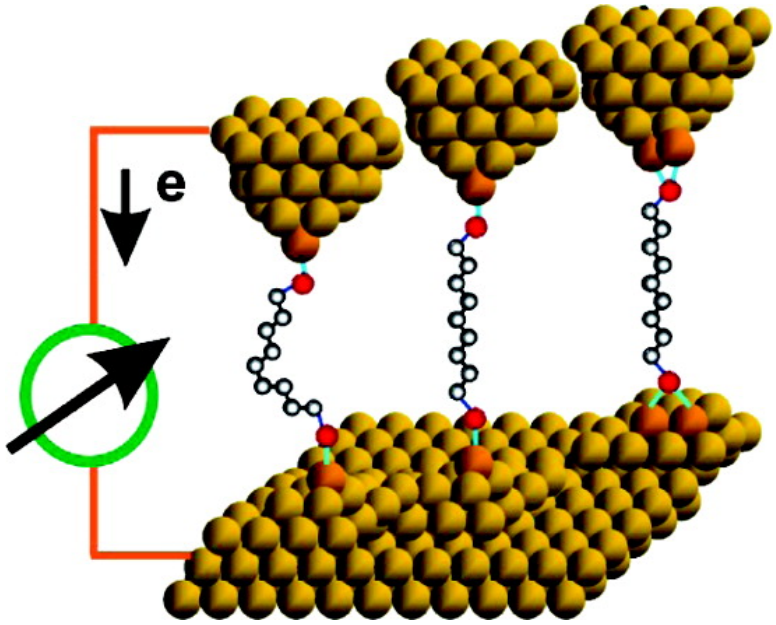

J|A|C|S
ARTICLES
Published on Web 12/13/2007

Charge Transport in Single Au | Alkanedithiol | Au Junctions: Coordination Geometries and Conformational Degrees of Freedom

Chen Li,[†,‡] Ilya Pobelov,[†,‡] Thomas Wandlowski,*[,†,‡] Alexei Bagrets,[§] Andreas Arnold,[§] and Ferdinand Evers*[,§,||]

Institute of Bio- and Nanosystems IBN 3 and Center of Nanoelectronic Systems for Information Technology, Research Center Jülich, D-52425 Jülich, Germany, Department of Chemistry and Biochemistry, University of Berne, CH-3012-Berne, Switzerland, Institute of Nanotechnology, Research Center Karlsruhe, P.O. Box 3640, D-76021 Karlsruhe, Germany, and Institut für Theorie der Kondensierten Materie, Universität Karlsruhe, 76021 Karlsruhe, Germany

Received August 21, 2007; E-mail: thomas.wandlowski@dcb.unibe.ch; Ferdinand.Evers@int.fzk.de

Abstract: Recent STM molecular break-junction experiments have revealed *multiple* series of peaks in the conductance histograms of alkanedithiols. To resolve a current controversy, we present here an in-depth study of charge transport properties of Au|alkanedithiol|Au junctions. Conductance histograms extracted from our STM measurements unambiguously confirm features showing more than one set of junction configurations. On the basis of quantum chemistry calculations, we propose that certain combinations of different sulfur−gold couplings and trans/gauche conformations act as the driving agents. The present study may have implications for experimental methodology: whenever conductances of different junction conformations are not statistically independent, the conductance histogram technique can exhibit a single series only, even though a much larger abundance of microscopic realizations exists.

Introduction

The ability to measure and control electrical currents through single molecules offers unique opportunities for exploring charge transport processes in tailored nanoscale junctions. Current approaches fall into the following three categories: scanning probe methods,[1−7] supported nanoelectrode assemblies[8−11] and mechanically controlled junctions, which have been refined so that gaps with even sub-angstrom resolution can be created using a piezo-electric transducer or other mechanical actuation mechanisms. Specific techniques include mechanically controlled break junctions (MCBJ[12−15]), STM and conducting AFM break junctions,[16,17] and STM-controlled point contact measurements.[18] The latter group of methods is particularly attractive because the technique is applicable to different environments, such as gas and solution phases as well as UHV conditions. Approaches differ in the following criteria: (i) formation of reproducible contacts between a molecule and two probing electrodes, (ii) access to "signatures" of single molecules, and (iii) details of statistical data analysis.

In order to improve experimental reproducibility, Xu and Tao[16] have begun to analyze the statistical properties of conductance traces, which show the conductance over a control parameter, measuring the electrode separation. Such current−distance traces were obtained from a repeated formation and breaking of a large number of individual molecular junctions formed between a gold STM tip and a gold substrate in a solution containing molecules.[16] The procedure was adopted and

[†] Research Center Jülich.
[‡] University of Bern.
[§] Research Center Karlsruhe.
[||] Universität Karlsruhe.

(1) Mazur, U.; Hipps, K. W. *J. Phys. Chem. B* **1999**, *103*, 9721−9727.
(2) Bumm, L. A.; Arnold, J. J.; Cygan, M. T.; Dunbar, T. D.; Burgin, T. P.; Jones, L.; Allara, D. L.; Tour, J. M.; Weiss, P. S. *Science* **1996**, *271*, 1705−1707.
(3) Andres, R. P.; Bein, T.; Dorogi, M.; Feng, S.; Henderson, J. I.; Kubiak, C. P.; Mahoney, W.; Osifchin, R. G.; Reifenberger, R. *Science* **1996**, *272*, 1323−1325.
(4) Cui, X. D.; Primak, A.; Zarate, X.; Tomfohr, J.; Sankey, O. F.; Moore, A. L.; Moore, T. A.; Gust, D.; Harris, G.; Lindsay, S. M. *Science* **2001**, *294*, 571−574.
(5) Ramachandran, G. K.; Tomfohr, J. K.; Li, J.; Sankey, O. F.; Zarate, X.; Primak, A.; Terazono, Y.; Moore, A. L.; Moore, T. A.; Gust, D.; Nagahara, L. A.; Lindsay, S. M. *J. Phys. Chem. B* **2003**, *107*, 6162−6169.
(6) Nazin, G. V.; Qiu, X. H.; Ho, W. *Science* **2003**, *302*, 77−81.
(7) Repp, J.; Meyer, G.; Paavilainen, S.; Olsson, F. E.; Persson, M. *Science* **2006**, *312*, 1196−1199.
(8) Park, J.; Pasupathy, A. N.; Goldsmith, J. I.; Chang, C.; Yaish, Y.; Petta, J. R.; Rinkoski, M.; Sethna, J. P.; Abruna, H. D.; McEuen, P. L.; Ralph, D. C. *Nature* **2002**, *417*, 722−725.
(9) Li, X. L.; He, H. X.; Xu, B. Q.; Xiao, X. Y.; Nagahara, L. A.; Amlani, I.; Tsui, R.; Tao, N. J. *Surf. Sci.* **2004**, *573*, 1−10.
(10) Kervennic, Y.; Thijssen, J. M.; Vanmaekelbergh, D.; Dabirian, R.; Jenneskens, L. W.; Walree, C. A. V.; van der Zant, H. S. J. *Angew. Chem., Int. Ed.* **2006**, *45*, 2540−2542.
(11) Dadosh, T.; Gordin, Y.; Krahne, R.; Khivrich, I.; Mahalu, D.; Frydman, V.; Sperling, J.; Yacoby, A.; Bar-Joseph, I. *Nature* **2005**, *436*, 677−680.
(12) Muller, C. J.; van Ruitenbeek, J. M.; de Jongh, L. J. *Phys. Rev. Lett.* **1992**, *69*, 140−143.
(13) Reed, M. A.; Zhou, C.; Muller, C. J.; Burgin, T. P.; Tour, J. M. *Science* **1997**, *278*, 252−254.
(14) Kergueris, C.; Bourgoin, J. P.; Palacin, S.; Esteve, D.; Urbina, C.; Magoga, M.; Joachim, C. *Phys. Rev. B.* **1999**, *59*, 12505−12513.
(15) Reichert, J.; Ochs, R.; Beckmann, D.; Weber, H. B.; Mayor, M.; von Löhneysen, H. *Phys. Rev. Lett.* **2002**, *88*, 176804.
(16) Xu, X. B.; Tao, N. J. *Science* **2003**, *301*, 1221−1223.
(17) Xu, X. B.; Xiao, X. Y.; Tao, N. J. *J. Am. Chem. Soc.* **2003**, *125*, 16164−16165.
(18) Haiss, W.; Zalinge, H. V.; Higgins, S.; Bethell, D.; Höbenreich, H.; Schiffrin, D.; Nichols, R. J. *J. Am. Chem. Soc.* **2003**, *125*, 15294−15295.

10.1021/ja0762386 CCC: $40.75

modified by several other groups.[18−26] The statistical interpretation of the individual conductance-distance traces is mostly based on the analysis of conductance plateaus[16,18,19,23,25] that leads to the construction of conductance histograms. Alternative approaches involve the logarithmic analysis of entire transients[21,27,28] or the rapid conductance drop in the last step.[22]

Despite using the statistical analysis and comparable experimental techniques, Tao et al.[16] and Haiss et al.[29] obtained qualitatively different traces for the average conductance $G(n)$ of an n-alkanedithiol: while ref 16 reports an exponential dependence $G(n) \sim \exp(-\beta_N n)$ with $\beta_N \approx 1$, data in ref 29 were represented by an exponential law, with $\beta_N = 0.52$, and are smaller by more than an order of magnitude. Slowinski et al.[25] also confirmed the exponential behavior. They found $\beta_N \approx 0.83$. However, after refinement of their measurement technique, Tao, Lindsay, and co-workers report[30] that, in fact, the conductance histogram analysis would not yield a unique trace $G(n)$ but rather two traces, none of them coinciding with the experiment by Haiss et al.[29] According to Fujihira et al.,[23] this result is still incomplete; even a third trace should exist.

The experimental controversy may seem surprising at first sight, since actually the stretched (trans configuration) alkane wire is a reasonably simple system; it has an even number of electrons per unit cell and thus is a band insulator. Since the alkane work function is only ~2 eV below the gold Fermi energy (E_F), while the alkane's conduction band is more than 5 eV above (according to our calculations, see below), the coupled wire shows HOMO-mediated transport. The tunneling barrier height Φ_B is given by the energy difference of E_F and the wire's upper valence band edge: $\Phi_B = E_F - E^*_{HOMO}$.

The variability of experimental results reflects fluctuations in the microscopic junction conditions. Therefore, variations in the metal-electrode contact geometry[21,30,31] and isomeric structures[29,32] (*gauche* conformations) have been put forward as an explanation for the appearance of multiple experimental conductance traces. However, it is clear that such an explanation is rather incomplete. Experimentally, a great many combinations of contact/isomeric degrees of freedom could exist, and in the case of the alkanes a substantial fraction of them should contribute to the transport characteristics. Since such junction modifications might be expected to exhibit conductances somewhat different from each other, it is in fact a nontrivial observation and an intriguing open question as to why equally spaced peak structures in the conductance histograms can appear at all.

This contribution constitutes an attempt to resolve this puzzle and to present a unifying view. We report an experimental STM study that establishes the existence of at least three series of peaks in conductance histograms of α,ω-alkanedithiols. On the basis of ab initio simulations of the single-molecule conductance, we will argue that many junction configurations add to the conductance histograms, as expected. Furthermore, our calculations also show that conductances of different junction conformations are correlated and in fact cluster at roughly integer multiples of some basic units. For this reason the equally spaced peak structures in conductance histograms are not smeared out. This illustrates an important conceptual consequence; in contrast to a widespread practice, a single peak sequence cannot necessarily be attributed to a specific junction configuration but rather it also can—and in the case of the alkanes it does—result from averaging over many junction configurations.

Experimental Section

Chemicals. The α,ω-alkanedithiols 1,5-pentanedithiol (PD), 1,6-hexanedithiol (HD), 1,8-octanedithiol (OD), 1,9-nonanedithiol (ND), and 1,10-decanedithiol (DD) were purchased from Aldrich (reagent grade) and used without further purification. The electrolyte solutions were prepared with Milli-Q water (18 MΩ, 2 ppb TOC) and HCl (35%, Merck suprapure). Absolute ethanol (KMF 08-205) and 1,3,5-trimethylbenzene (TMB, p.a. 98%) were obtained from KMF Laborchemie Handels GmbH and Sigma-Aldrich, respectively.

Electrode and Sample Preparation. The Au(111) electrodes used in this work were discs of 2 mm height and 10 mm in diameter, nominal miscut <0.1°. Island-free Au(111)-(1 × 1) surfaces were prepared by immersing a flame-annealed Au(111)-($p \times \sqrt{3}$) electrode into deareated 0.05 M HCl for 20 min.[33] The electrode was then immersed, rinsed with absolute ethanol, and dried in a stream of argon.

The organic adlayers were prepared by immersing the dry Au(111)-(1 × 1) electrode into a 0.1 mM ethanolic solution of the respective α,ω-alkanedithiol for 2 min. Subsequently, the modified electrodes were removed from the assembly solution, rinsed with warm ethanol, transferred into the STM cell, and covered with TMB. Selected experiments were carried out directly in 0.1 mM TMB solutions of the α,ω-alkanedithiols.

Single-Junction Conductance Measurements. The STM imaging and the STS (current−distance) measurements were carried out sequentially at room temperature in 1,3,5-trimethylbenzene (TMB) using a modified Molecular Imaging PicoSPM. The STM tips were uncoated, electrochemically etched gold wires (99.999%, 0.25 mm diameter, etching solution 1:1 mixture of 30% HCl and ethanol).[34] All STM measurements were conducted in a sealed container, to prevent oxygen exposure, and in constant current mode employing low tunneling currents (10−100 pA), and bias voltages E_{bias} ranging between ±0.010 and ±0.300 V.

Single-junction conductance data were obtained from current−distance traces employing either a single-channel preamplifier (0.1, 1.0, or 10 nA/V) or a dual multichannel preamplifier stage capable of recording currents in 1 pA ≤ i_T ≤ 210 μA simultaneously.[35] The latter was combined with a customized control circuit and a multichannel scope recorder Yokogawa DL 750 (1 MS s^{-1}, 16 bit). The following sequence (Figure 1) was applied. A sharp, gold STM tip, capable of

(19) Li, Z.; Han, B.; Meszaros, G.; Pobelov, I.; Wandlowski, Th.; Blaszczyk, A.; Mayor, M. *Faraday Discuss.* **2006**, *131*, 121−143.
(20) Chen, F.; He, J.; Nuckolls, C.; Roberts, T.; Klare, J.; Lindsay, S. M. *Nano Lett.* **2005**, *5*, 503.
(21) Ulrich, J.; Esrail, D.; Pontius, W.; Venkataraman, L.; Millar, D.; Doerrer, L. H. *J. Phys. Chem. B* **2006**, *110*, 2462−2466.
(22) Jang, S. Y.; Reddy, P.; Majumdar, A.; Segalman, R. A. *Nano Lett.* **2006**, *6*, 2362−2367.
(23) Fujihira, M.; Suzuki, M.; Fujii, S.; Nishikawa, A. *Phys. Chem. Chem. Phys.* **2006**, *8*, 3876−3884.
(24) Sek, S.; Misicka, A.; Swiatek, K.; Maicka, E. *J. Phys. Chem.* **2006**, *110*, 19671−19677.
(25) Wierzbinski, E.; Slowinski, K. *Langmuir* **2006**, *22*, 5205−5208.
(26) Li, Z.; Pobelov, I.; Han, B.; Wandlowski, Th.; Blaszczyk, A.; Mayor, M. *Nanotechnology* **2007**, *18*, 044018.
(27) Venkataraman, L.; Klare, J. E.; Nuckolls, C.; Hybertsen, M. S.; Steigerwald, M. L. *Nature* **2006**, *442*, 904−907.
(28) Gonzalez, M. T.; Wu, S.; Huber, R.; van der Molen, S. J.; Schönenberger, C.; Calame, M. *Nano Lett.* **2006**, *6*, 2238−2242.
(29) Haiss, W.; Nichols, R. J.; van Zalinge, H.; Higgins, S. J.; Bethell, D.; Schiffrin, D. J. *Phys. Chem. Chem. Phys.* **2004**, *6*, 4330−4337.
(30) Li, X.; He, J.; Hihath, J.; Xu, B.; Lindsay, S. M.; Tao, N. J. *J. Am. Chem. Soc.* **2006**, *128*, 2135−2141.
(31) Müller, K. H. *Phys. Rev. B* **2006**, *73*, 045403.
(32) Haiss, W.; van Zalinge, H.; Bethell, D.; Ulstrup, J.; Schiffrin, D. J.; Nichols, R. J. *Faraday Discuss.* **2006**, *131*, 253−264.
(33) Hölzle, M. H.; Wandlowski, Th.; Kolb, D. M. *J. Electroanal. Chem.* **1995**, *394*, 271−275.
(34) Ren, B.; Piccardi, G.; Pettinger, B. *Rev. Sci. Instrum.* **2004**, *75*, 837−841.
(35) Meszarosz, G.; Li, C.; Pobelov, I.; Wandlowski, Th. *Nanotechnology* **2007**, *18*, 424004.

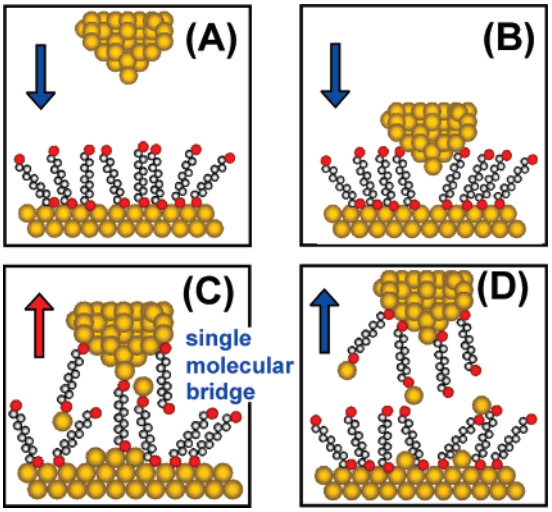

Figure 1. Schematic representation of the STM-type contact junction approach applied in the present study. (A) Approach, (B) formation of molecular contacts, (C) pulling, and (D) breaking.

imaging experiments with atomic resolution, was brought to a preset tunneling position, typically defined by i_T = 50 or 100 pA and E_{bias} ranging between ±0.010 V and ±0.300 V (Figure 1A). Subsequently, the STM feedback was switched off, and the tip approached the adsorbate-modified substrate surface at constant $x-y$ position (Figure 1B). The approach was stopped before reaching point contact with the gold surface ("gently touch") by choosing an upper threshold current of 0.2 G_0E_{bias} (G_0 = 77.5 μS). These settings still ensure rather strong interactions between the gold tip and the α,ω-alkanedithiol adlayer. After a dwelling time of 100 ms, sufficient to create molecular junctions between tip and substrate, the tip was retracted with a rate of 5−10 nm s^{-1} until a lower threshold position was reached. The latter was chosen sufficiently far from the adsorbate-modified substrate to ensure the breaking of all Au|α,ω-alkanedithiol|Au junctions. This process may also involve the attachment/detachment and/or reorganization of gold adatoms[17,19,36,37] The transient conductance curves were recorded, and the entire cycle was repeated up to 3000 times.

We notice that the experimental technique applied in the present study exhibits a distinct difference compared to the original approach reported by Xu et al. in ref 16. The choice of a single or dual preamplifier stage with a wide dynamic range and coupled with a highly sensitive feedback loop[35] ensured that no physical contact between gold tip and gold substrate occurred prior to the formation of molecular junctions. This new technical development increased stability and reproducibility of the single molecular junction studies with alkanedithiols significantly. The "gentle touch" technique does not lead to major modifications of the STM tip due to tip crashes. In consequence, the adsorbate-covered surface could always be monitored between cycles of current−distance traces with a high-quality tip capable of molecular resolution.

Results

Figure 2A illustrates, as an example, the typical response of the simultaneously recorded high- and low-current channels during a complete approaching/retracting cycle for 0.1 mM 1,9-nonanedithiol (ND) in TMB. The upper limit current of 1.5 μA, as monitored in the high-current channel, prevents the formation of Au−Au nanocontacts. STM images, recorded with the same gold tip before and after the transient conductance trace, are

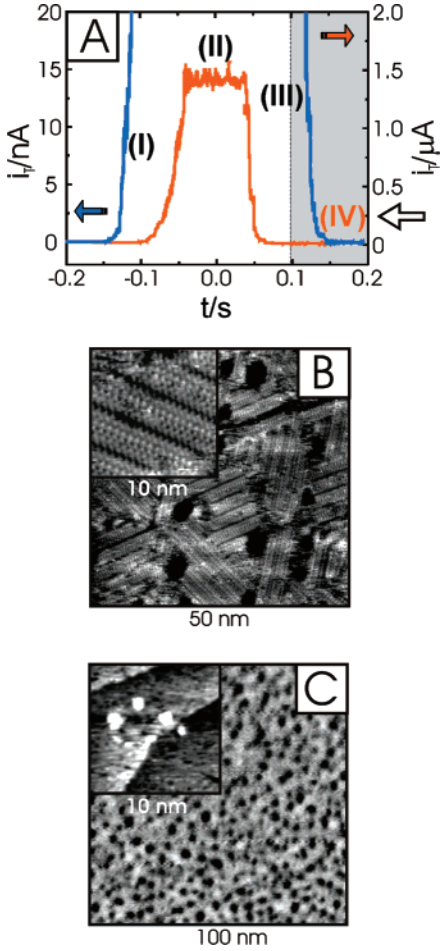

Figure 2. (A) Simultaneously recorded current vs time traces of a complete approaching and breaking cycle for 0.1 mM 1,9-nonanedithiol (ND) in 1,3,5-trimethylbenzene (TMB). The symbols of the individual steps follow the nomenclature of Figure 1. The orange trace represents the high-current channel (maximum range 3 nA < i_T ≤ 23 μA), which monitors the exact position of the tip relative to the substrate surface. Typically, we stopped the z movement of the tip upon reaching a current between 1 and 2 μA. The orange trace refers to $i_T \approx$ 1.5 μA. The blue trace illustrates the low-current channel (10 pA < i_T < 35 nA), which is chosen to follow single-junction conductance characteristics. (B) Large scale and high-resolution (inset) STM images of the striped low-coverage phase (i_T = 0.1 nA; E_{bias} = 0.1 V) of ND on Au(111)-(1 × 1) in TMB monitored with a gold STM tip before and during a sequence of stretching experiment. (C) Large scale image of the disordered high-coverage phase of ND on Au(111)-(1 × 1), other conditions identical to those of (B). The adlayers are typically unaltered. Only occasionally did we observe the formation of small, monatomically high gold islands.

identical, exhibiting either an ordered low-coverage striped phase (Figure 2B) or a disordered high-coverage phase with characteristic vacancy islands (Figure 2C) depending on the initial assembly conditions. Occasionally, a few monatomic gold islands were observed after a long series of current−distance traces (cf. inset in Figure 2C).

The retraction or pulling curves were recorded with high resolution in 1 pA < i_T < 100 nA. We observed three types of transient curves. Type I curves are exponential and represent direct electron tunneling between the gold tip and the substrate without molecular junctions being formed.[26,30] The percentage of these decay curves was 50% when performing the experiment in TMB containing 0.1 mM ND, and up to 80% in the presence of an ND adlayer without molecules being dissolved in electrolyte. Assuming a rectangular barrier, we estimated at large

(36) Yu, M.; Bovet, N.; Satterley, C. J.; Bengio, S.; Lovelock, K. R. J.; Milligan, P. K.; Jones, R. G.; Woodruff, D. P.; Dhanak, V. *Phys. Rev. Lett.* **2006**, *97*, 166102.
(37) Grönbeck, H.; Häkkinen, H. *J. Phys. Chem. B* **2007**, *111*, 3325−3327.

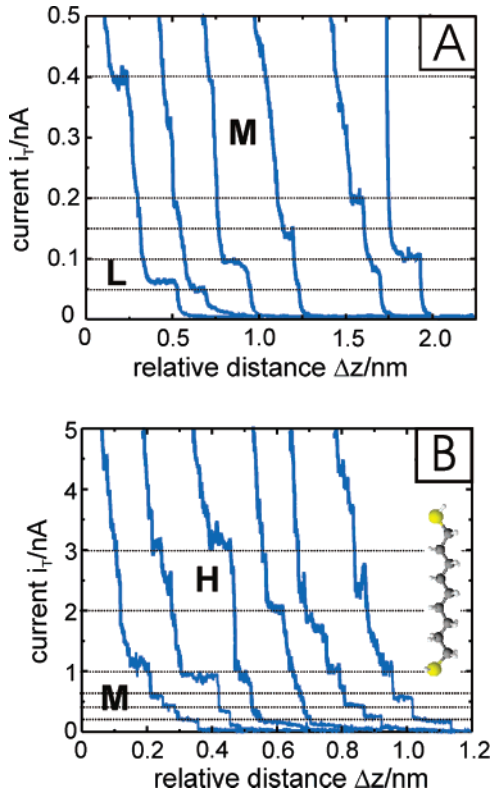

Figure 3. (A) Current−distance retraction curves recorded with a gold STM tip (low-current channel with a preamplifier limit of 1 nA) for 0.1 mM 1,9-nonanedithiol in 1,3,5-trimethylbenzene on Au(111)-(1 × 1), at E_{bias} = 0.10 V. The setpoint current before disabling the feedback was chosen at i_0 = 100 pA. The pulling rate was 4 nm s^{-1}. (B) Same conditions as in (A), except that the preamplifier limit was chosen at 10 nA. The dotted lines represent characteristic regions of the low, mid, and high currents. For further explanation we refer to the text.

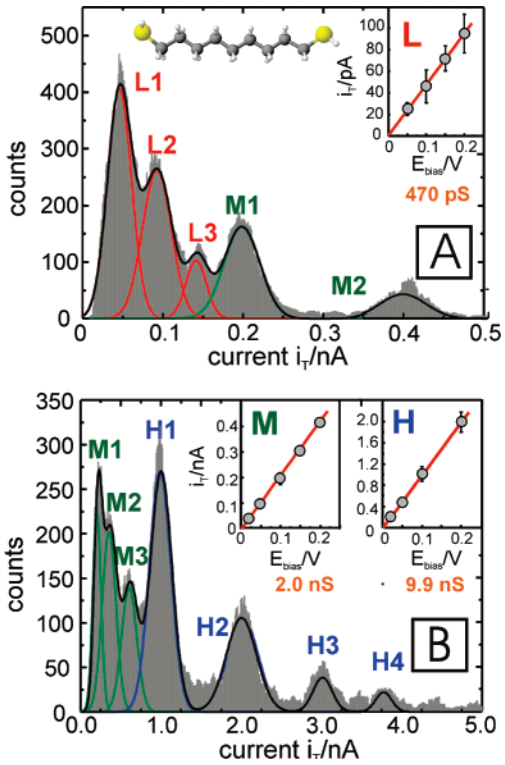

Figure 4. Conductance histograms constructed from values of the plateaus of type III "stretching" curves for Au|1,9-nonanedithiol|Au junctions. (A) 1600 out of 4300 traces employing the 1 nA (max) preamplifier; (B) 1100 out of 4300 traces recorded with the 10 nA (max) preamplifier. All other conditions are identical to those in Figure 3. We notice that the low-conductance sequence could only be resolved with the high sensitive preamplifier. Insets in (A) and (B) show that the current within each series scales *approximately* linearly with the bias voltage.

tip-adsorbate distances an effective barrier height Φ_{eff} = (1.1 ± 0.2) eV, which is comparable with data obtained for the bare gold|TMB system.[38] Type II curves are nonmonotonic and noisy, which could be attributed to mechanical instabilities. The percentage of these curves was around 10%. Traces of type I and II were rejected in the further analysis of the experimental data. The remaining type III conductance traces are monotonic and non-exponential. Figure 3 illustrates typical examples for 0.1 mM ND in TMB recorded with preamplifier settings of 0.1 nA V^{-1} (A) and 1.0 nA V^{-1} (B) for the low-current channel. They exhibit single plateaus or series of plateaus with a typical length of 0.04−0.15 nm, which are separated by abrupt steps of 50 pA up to 3 nA. These current steps are assigned to the breaking of individual respective multimolecular ND junctions previously formed between the gold STM tip and the substrate surface.[26,30] The percentage of type III conductance traces varied between 40% and 10%, depending if ND is dissolved in TMB or only pre-adsorbed on the Au(111)-(1 × 1) surface. Similar observations were reported previously by Li et al.[30] Control experiments in pure TMB displayed almost exclusively (98%) exponentially decaying traces. No evidence of current steps resembling type III traces was found.

The statistical analysis of type III conductance traces was carried out by constructing histograms, typically based on up to 1500 individual curves. We have chosen a numerical routine, which selects plateau currents according to the following criteria[19,38]: minimum plateau length of 0.04 nm and an average variation of the current magnitude of less than 5%. Figure 4 displays two histograms that were obtained from two experiments with 0.1 mM ND in TMB under conditions illustrated in Figure 3. An analysis of the characteristic conductance peaks allows identifying three different sequences of equally spaced maxima. They are attributed to low, L, medium, M, and high, H, conductance junctions. The current within each series scales *approximately* linearly with the number of peaks. The first peak of each sequence is attributed to a single molecular junction. The corresponding currents depend also linearly on the applied bias voltage, at least up to ±0.200 V (cf. insets in A and B of Figure 4). These correlations lead to the following conductance values of the three specific single-molecule Au|ND|Au junctions: (0.47 ± 0.03) nS (L), (2.0 ± 0.2) nS (M) and (9.9 ± 0.9) nS (H). We obtained the same results when constructing all-data-point histograms (cf. Figure S1 in the Supporting Information). A comprehensive discussion of advantages and pitfalls of different approaches for the construction of conductance histograms will be presented in a forthcoming paper.[38]

Following the same experimental protocol we obtained also multipeak conductance histograms for 1,5-pentanedithiol (PD), 1,6-hexanedithiol (HD), 1,8-octanedithiol (OD), and 1,10-decanedithiol (DD) in TMB. The respective data of the single-junction conductances are summarized in Table 1.

The values of the H conductance are approximately a factor of 5 larger compared to the M conductance for the same

(38) Pobelov, I.; Li, C.; Meszarosz, G.; Wandlowski, Th. *Small* **2007**. Manuscript in preparation.

Table 1. Single Junction Conductance Data Au|α,ω-Alkanedithiol|Au

	conductance (nS)		
α,ω-alkanedithiol	L	M	H
PD ($n = 5$)	1.9 ± 0.05	64 ± 5	–
HD ($n = 6$)	2.45 ± 0.06	20 ± 2	95 ± 10
OD ($n = 8$)	0.89 ± 0.08	4.4 ± 0.4	21 ± 2
ND ($n = 9$)	0.47 ± 0.03	2.0 ± 0.2	9.9 ± 0.9
DD ($n = 10$)	0.22 ± 0.02	0.45 ± 0.04	1.68 ± 0.03

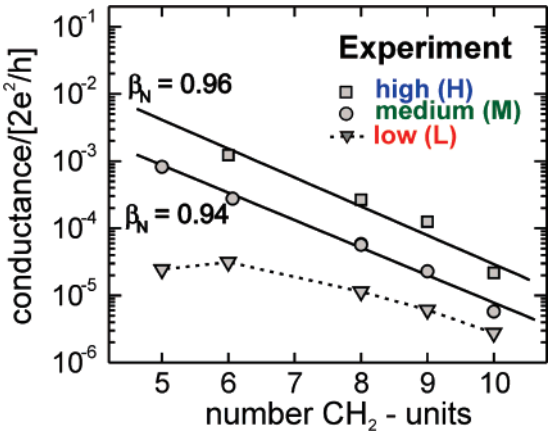

Figure 5. Chain-length dependence of the single-junction Au | alkanedithiol | Au conductivity in a semilogarithmic representation. The three sets of conductance values—high (H), medium (M) and low (L)—are shown as squares, circles, and triangles. The straight lines were obtained from a linear regression analysis with decay constants β_N defined per methylene (CH_2) unit.

molecule, while the lowest values L do not scale with a constant ratio. The M and L conductance data approach each other with increasing chain length. As an example, we refer to M(PD):L(PD) ≈ 34 and M(DD):L(DD) ≈ 2. Furthermore, we found that the single-junction conductance data of the three sequences are rather independent of alkanedithiol concentration and coverage. No preferential occurrence of H, M, or L conductance junctions was observed for the aliphatic molecules studied. However, within one sequence one could typically resolve up to three peaks with a distinct preference for single molecular junctions. Integration yields an average ratio of 0.54:0.35:0.11 to form one-, two- or three-molecule junctions.

We also note that the H and M values of the single-junction conductance for HD, OD, and DD, as obtained in the present study, are in agreement with data recorded after breaking preformed Au−Au nanocontacts in toluene containing 1.0 mM solutions of the respective alkanedithiols.[16,22,30] The mid-conductance of a single molecular Au|OD|Au junction is supported by experiments of Gonzalez et al.,[28] who carried out a MCBJ experiment in a liquid cell filled with 1 mM OD in TMB. The values of the L conductance of HD, OD, and ND are comparable with data reported by Haiss et al. in air and toluene as well as under electrochemical conditions.[29,32] No agreement was found between the results of our study and the STM-based single-molecule conductance measurements of Fujihira et al. carried out under UHV conditions for Au|HD|Au.[23]

Figure 5 shows the semilogarithmic plot of the conductance versus molecular length. The latter being expressed as the number of CH_2 units. The H and M conductance values follow a simple tunneling model given by $G = G_c \cdot \exp(-\beta_N \cdot n)$ with decay constants β_N of (0.96 ± 0.15) and (0.94 ± 0.05),

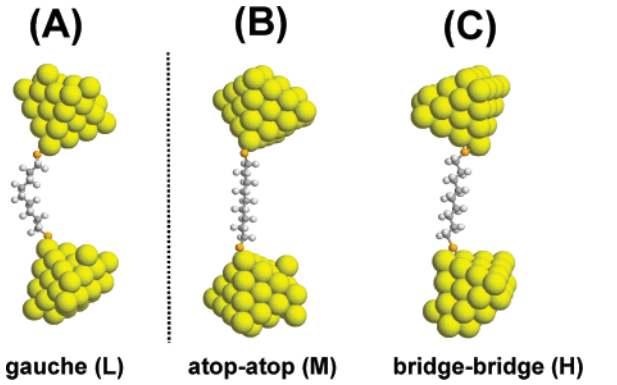

Figure 6. Three typical arrangements of a single alkanedithiol molecule bridged between Au electrodes as used for the conductance calculations. (A) 1,9-Nonanedithiol (ND) with one gauche defect and both terminal sulfur atoms coordinated in the atop position (low, L). (B) ND in all-trans conformation and in atop−atop coordination (medium, M). (C) All-trans ND in a bridge−bridge coordination (high, H).

respectively. These values of β_N are in agreement with literature data on the M and/or H conductances of single-junction Au|alkanedithiol|Au[16,22,30] as well as for the electron transfer through compact and aligned monolayers of alkanethiols using nanopores,[39] mercury contacts,[40,41,42] CP-AFM,[43] or redox probes.[44,45]

The low-conductance data give a rather poor linear correlation with a decay constant $\beta_N \approx (0.45 \pm 0.09)$, distinctly different from the H and M sequences. However, we notice that the estimated value β_N is rather close to that reported by Haiss et al.[29]

Theoretical Section

Model and Method. To provide insight into the multi-peak series observed experimentally, we have performed DFT-based calculations of alkanedithiols coupled to Au electrodes, using a standard quantum chemistry package TURBOMOLE.[46] Calculations were done for different configurations of an "*extended molecule*" composed of an *n*-alkanedithiol of variable chain lengths ($n = 4, ..., 10$) bridged between two pyramids of ~40 ÷ 55 Au atoms (Figure 6). These clusters model the contact region of the gold electrodes. We employed the generalized gradient approximation (GGA, BP86 functional[47]) with a contracted Gaussian-type basis set of triple-ζ valence quality including polarization functions.[48] The experimental lattice constant of 4.08 Å was fixed for bulk fcc-Au clusters, whereas relaxed configurations were found for the alkanedithiol mol-

(39) Wan, W. Y.; Lee, T.; Reed, M. A. *Phys. Rev. B* **2003**, *68*, 0354161.
(40) Slowinski, K.; Chamberlain, R. V.; Miller, C. J.; Majda, M. *J. Am. Chem. Soc.* **1997**, *119*, 11910−11919.
(41) York, R. L.; Nguyen, P. T.; Slowinski, K. *J. Am. Chem. Soc.* **2003**, *125*, 5948−5953.
(42) Holmlin, R. E.; Haag, R.; Chabinyc, M. L.; Ismagilov, R. F.; Cohen, A. E.; Terfort, A.; Rampi, M. A.; Whitesides, G. M. *J. Am. Chem. Soc.* **2001**, *123*, 5075−5085.
(43) Wold, D. J.; Frisbie, C. D. *J. Am. Chem. Soc.* **2001**, *123*, 5549−5556.
(44) Chidsey, C. E. D. *Science* **1991**, *251*, 919−922.
(45) Smalley, J. F.; Feldberg, S. W.; Chidsey, C. E. D.; Linford, M. R.; Newton, M. N.; Liu, Y. P. *J. Phys. Chem.* **1995**, *99*, 13141−13149.
(46) (a) Treutler, O.; Ahlrichs, R. *J. Chem. Phys.* **1995**, *102*, 346−354. (b) Eichkorn, K.; Treutler, O.; Öhm, H.; Häser, M.; Ahlrichs, R. *Chem. Phys. Lett.* **1995**, *240*, 283−289; *Chem. Phys. Lett.* **1995**, *242*, 652−660. (c) Eichkorn, K.; Weigend, F.; Treutler, O.; Ahlrichs, R. *Theor. Chem. Acc.* **1997**, *97*, 119−124. (d) Sierka, M.; Hogekamp, A.; Ahlrichs, R. *J. Chem. Phys.* **2003**, *118*, 9136−9148.
(47) (a) Becke, A. D. *Phys. Rev. A* **1988**, *38*, 3098−3100. (b) Perdew, J. P. *Phys. Rev. B* **1986**, *33*, 8822−8824.
(48) Schäfer, A.; Huber, C.; Ahlrichs, R. *J. Chem. Phys.* **1994**, *100*, 5829−5835.

ecules coupled to few gold atoms assuming different gold−sulfur coordination geometries, namely: (i) S atop a Au atom (Figure 6A,B); (ii) S forming a bridge with two Au atoms (Figure 6C), or (iii) S placed in a (111) hollow site.[49] We obtained S−Au bond distances of 2.28, 2.36, and 2.72 Å for atop, bridge, and hollow-site configurations, respectively. We also considered all-trans and various gauche conformations of the alkyl chains. Conductances have been calculated within the Landauer approach, as implemented in a homemade simulation package.[50−52]

Results

Elementary Consideration of Transport Mechanism. To begin with, we consider all-trans isomers with the sulfur coupled to a single Au atom at each electrode (atop−atop geometry, Figure 6B). For the description of the electron transport, we consider the energy-dependent transmission $T(E)$ (Figure 7A). It represents the probability for electrons injected with the energy E from one electrode to be transmitted through the molecular junction. The conductance is defined by the transmission $T(E_F)$ evaluated at the Fermi energy (E_F) in units of the conductance quantum $G_0 = 2e^2/h = 77.5\ \mu$S. Molecular states of alkanedithiols appear as resonance peaks in the transmission spectrum (see Figure 7A).

Our findings fully support the qualitative picture of transport through alkanes outlined in the introduction. The Fermi energy E_F is situated inside the alkane HOMO−LUMO gap (7.5 eV in the present calculations) giving rise to an effective barrier $\Phi_B = E_F - E^*_{HOMO} = 2.14$ eV. The current flow involves mainly the alkane-HOMO (HOMO* of the alkanedithiol) depicted in Figure 7A (insert). Accordingly, the transmission $T(E)$ drops down rapidly around −2.2 eV below E_F and a nearly insulating gap spreads up all the way until 5.3 eV above E_F (alkane-LUMO, Figure 7A). Furthermore, the conductance through n-alkanedithiol junctions decays exponentially according to $G(n) = G_c \exp(-\beta_N n)$ with a decay constant $\beta_N \propto \Phi_B^{1/2} d_0$, where $d_0 = 1.28$ Å is the unit length of the alkane chain. We found $\beta_N = 0.83$ per CH_2 unit (open circles in Figure 8A). A value $G_c = 0.24G_0 = 18.5\ \mu$S was obtained for the contact conductance.

So far, our analysis has not yet included the thiol end-groups. They introduce two evanescent gap states built of symmetric and antisymmetric combinations of wave functions localized at the *sulfur* atoms (Figure 7B, inset). These states appear as broad resonances centered around $E_S \approx -1.4$ eV below E_F in the transmission spectrum (see Figure 7B). To describe such a

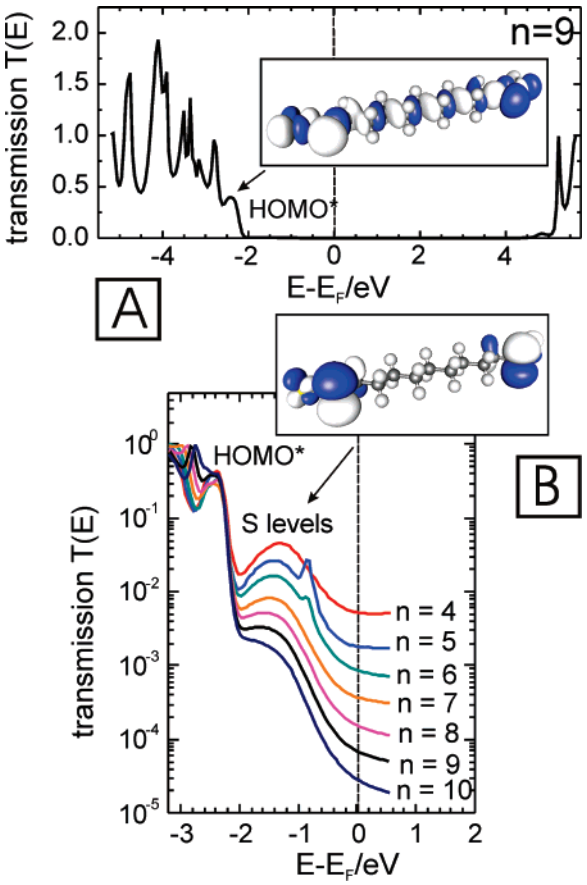

Figure 7. (A) Calculated energy-dependent transmission $T(E)$ for a single 1,9-nonanedithiol molecule ($n = 9$) bridged between gold electrodes in an all-trans atop−atop arrangement (panel B in Figure 6). (Inset) Molecular orbital of the Au−S−$(CH_2)_9$−S−Au cluster, formed by the nonane HOMO hybridized with the S and the Au electronic levels. This state determines the tunneling barrier. (B) Energy-dependent transmissions of the n-alkanedithiols of various lengths n around the Fermi level. (Inset) Alkanedithiol's HOMO, which is an antisymmetric superposition of atomic wave functions localized on both sulfur atoms. The energy difference within its symmetric part, HOMO-1, is exponentially decaying with n.

situation, we apply the Breit−Wigner formula,[53] $T(E) = 2\Gamma_S \gamma_n(E)/[(E - E_S)^2 + (\Gamma_S + \gamma_n(E))^2/4]$. Here, Γ_S denotes an on-resonance probability amplitude (inverse lifetime) for an electron to hop from the S atom to the nearest electrode. From our data we obtain $\Gamma_S = 1.25$ eV. The other probability $\gamma_n(E) \ll \Gamma_S$ reflects tunneling through the molecule and is exponentially small, $\gamma_n(E) = \gamma_0 \exp[-\beta(E)n]$, where $\beta(E) \propto [E - E^*_{HOMO}]^{1/2} d_0$. The tails of such broad peaks, when approaching the Fermi energy (Figure 7B), define the amplitude of the molecular conductance $G(n) \cong 2G_0\Gamma_S\gamma_0 \exp[-\beta(E_F)n]/(E_F - E_S)$.[2] Notice that an evanescent state localized close to an Au surface does not change the tunneling asymptotics, which is defined by an offset of the alkane HOMO state (E^*_{HOMO}) with respect to E_F, since $\beta(E_F) = \beta_N$.

Effect of Contact Geometry. The effect of contact geometry has been appreciated by many authors.[31,50,54−56] Figure 8A clearly shows, that many contact configurations exhibit com-

(49) As shown in ref 50, in case of sulfur bound to a plane Au(111) surface, the hollow site is the most stable one, the "bridge" geometry corresponds to a local minimum of free-energy, while the "atop" position is, in fact, unstable. However, in the case of a corrugated surface, near the edges, the "bridge" geometry is the most preferable one, the "atop" position remains at a local minimum in energy, and the hollow site is unstable. Thus, it is worth considering all three cases. Note that even in flat-surface experiments (essentially no surface reconstruction), sulfur does not usually bind to hollow sites but rather prefers binding to Au adatoms, as has been shown in ref 36.

(50) Evers, F.; Weigend, F.; Köntopp, M. *Phys. Rev. B* **2004**, *69*, 235411.

(51) (a) Evers, F.; Arnold, A. cond-mat/0611401. (b) Arnold, A.; Weigend, F.; Evers, F. *J. Chem. Phys.* **2007**, *126*, 1740−1746.

(52) We describe the interaction between the "extended molecule" and the rest of semi-infinite electrodes via an efficient approximation for the self-energy, represented by a local leakage function, $\Sigma(\mathbf{r},\mathbf{r}') \approx i\eta\delta(\mathbf{r} - \mathbf{r}')$ (please, see ref 51 for details). To improve convergence with the number of Au contact atoms, we use chaotic contact cavities produced by adding few adatoms to otherwise symmetric Au pyramids. Then the value of the level broadening η can be varied by one order of magnitude (around ∼0.1 Hartree in the present case), leaving the results for the transmission unchanged within a few percent.

(53) Vedyayev, A.; Bagrets, D.; Bagrets, A.; Dieny, D. *Phys. Rev. B* **2001**, *63*, 064429.

(54) Grigoriev, A.; Sköldberg, J.; Wendin, G.; Crljen, Z. *Phys. Rev. B* **2006**, *74*, 045401.

(55) Kondo, H.; Kino, H.; Nara, J.; Ozaki, T.; Ohno, T. *Phys. Rev. B* **2006**, *73*, 235323.

(56) Ke, S. H.; Baranger, H. U.; Yang, W. *J. Chem. Phys.* **2005**, *123*, 114701.

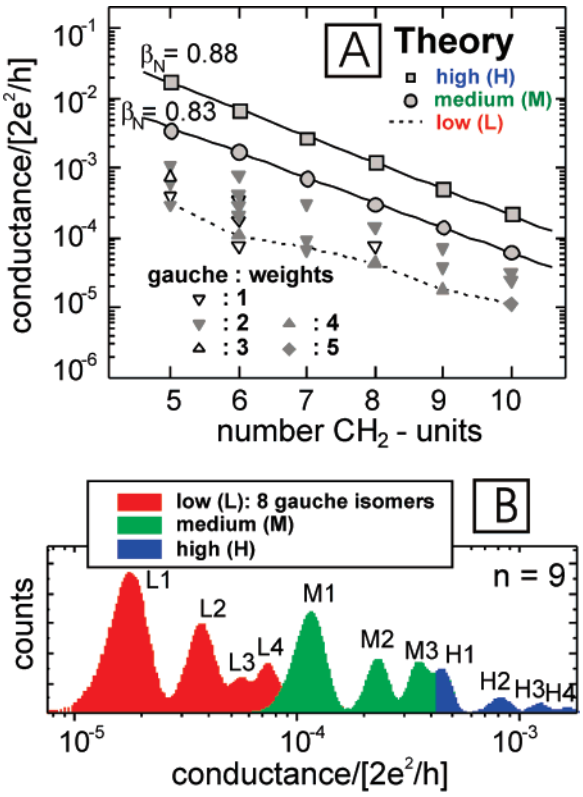

Figure 8. (A) Calculated conductance values of the Au|*n*-alkanedithiol|Au junctions vs number *n* of methylene units in a semilogarithmic representation. The straight lines are based on the linear regression analysis. The high (H, filled squares) and medium (M, filled circles) values were directly obtained for the arrangements of molecular bridges depicted in C and B of Figure 6. The conductances of many different, nonequivalent gauche isomers cover the window below the medium values. An alkyl chain obeys mirror symmetry. Therefore, depending on the position of the structural defect (cf. Figure 6A), different configurations can have the same conductances. Thus, statistical weights 1 or 2 can be ascribed to calculated values. Since some of the obtained values were very close to each other, weights up to 5 appeared as well. Namely, down-pointing open and filled triangles correspond to statistical weights 1 and 2. (B) Example of a simulated conductance histogram for a molecule with $n = 9$ units. Extracting the positions of the lowest conductance peaks leads to the dashed line drawn in A. Further details of the histogram construction are given in ref 59 (Supporting Information).

parable conductance values. The largest values (squares, Figure 8A) are associated with all-trans configurations and the sulfur bound to two Au atoms on either side (S−Au_2, bridge−bridge configuration, Figure 6C). For a double S−Au_1 contact configuration (atop−atop, Figure 6B) the conductance is reduced by a factor of 4, i.e., a factor of 2 per each anchoring group (circles, Figure 8A). The combination S−Au_2 on one side and S−Au_1 (bridge−atop) on the other predicts a factor of 2. A rationale for the factors of 2 per anchoring group is readily found by recalling that the number of escape channels per side doubles ($\Gamma_S \rightarrow 2\Gamma_S$), when the number of Au atoms connecting to the sulfur increases from 1 to 2.[57] In addition, we explored configurations with alkanedithiols embedded in short chains of gold adatoms (extended atop geometry). The resulting values of the junction conductances were changing within 10% only, and therefore such configurations do not need to be considered separately. Contradicting statements in the literature[58] according to which adatoms would change conductances of S−Au bonding molecules by an order of magnitude suffer heavily from modeling artifacts. Specifically, these earlier calculations assumed an unphysical angle of 180° of the Au−S−C angle, while the correct value used in our analysis is ∼104.5°.

Effect of Gauche Defects. We have repeated similar calculations for different gauche isomers. Because of the structural defect in the otherwise homogeneous potential barrier, they exhibit conductance values typically a factor ∼10 smaller than those of all-trans alkanedithiol chains (see Figure 8A, triangles). Also the different gauche isomers can be coupled to Au leads via different contact geometries. The net effect of the combined degrees of freedom, gauche, and contact geometry is that the molecular junctions with alkanedithiols can exhibit conductance values with a spreading of roughly 2 orders of magnitude.

Conductance Histograms. Referring to the above situation, it is not clear a priori, which result the experimentally used conductance histogram technique would actually show. We mimic the experimental approach and simulated conductance histograms to obtain a rough idea (Figure 8B). Essentially, we assume that all single-molecule contact configurations occur with equal probability and molecular bridges up to four molecules (trans or gauche conformations) can be formed. However, the probability of *n*-molecular junction to occur is suppressed by a factor of p^{n-1} where $p < 1$. In other words, we assume that the proability for a contact with two molecules in parallel is a factor of *p* lower than for a single-molecule contact, etc. We propose that thermodynamic fluctuations imply an incoherent averaging of conductance values associated with conformational and other environmental degrees of freedom. The associated peak broadening we model by a Gaussian distribution assigned to each calculated conductance value shown in Figure 8A (see ref 59 and Supporting Information for further details). We believe that as rough as our statistical model may be, its qualitative features are significant since they are not too much dependent on specific model assumptions.

The key result of this analysis is that three series of conductance peaks, L, M, and H, may be identified from the simulated conductance histograms (Figure 8B). The peak values are nearly equally spaced, neatly separated by integer multiples of some "master values". The L-series originates from gauche isomers. The M-series is due to all-trans molecules coupled to single Au atoms at one or both sides. The H-series comes from the all-trans isomers where both S atoms are coordinated with two Au atoms. Notice that the L-peaks do not strictly follow an exponential *n*-dependence, which is not surprising since they represent a convolution of many different junction conformations. By contrast, calculated middle (M)- and high (H)-conductance values fit to the exponential decay law with $\beta_N = 0.83-0.88$ per CH_2 unit.

Decay Constant β_N. The calculations of β_N were carried out using the generalized gradient approximation, GGA. In order to estimate the error related to the local character of GGA, we have performed additional calculations with a hybrid functional, B3LYP, which partly captures the long-range component of the exact functional that is completely absent in local approxima-

(57) We also checked the hollow−hollow configuration, even though it is not likely to be realized experimentally, see refs 36, 49. We found that the conductance was only a factor of ∼2 larger than the atop−atop configuration, which is caused by the increased sulfur−Au bond length.

(58) Di Ventra, M.; Pantelides, S. T., Lang, N. D. *Phys. Rev. Lett.* **2000**, *84*, 979−982.

(59) See Supporting Information.

tions. The calculation within the B3LYP functional[60] leads to an increase of the HOMO−LUMO gap for the pure alkane chains and to a shift of the alkane-HOMO down to −3.1 eV with respect to E_F that implies a higher tunneling barrier Φ_B. Since $\beta_N \propto \Phi_B^{1/2}$, the decay constant β_N increases from 0.83 to 1.0, as it should. Consistent with this observation, another hybrid functional, TPSSH,[61] also leads to an increased $\beta_N \approx 0.93$. On the basis of this error analysis, we believe that the exact value could be up to ∼20% larger than our GGA-based result.

The estimates based on a complex band structure analysis, performed by Tomfohr and Sankey,[62] and by Picaud et al.,[63] suggested $\beta_N \approx 1.0$ and ≈ 0.9 respectively, in agreement with our findings. Their estimates for the tunneling barrier $\Phi_B \approx 3.5 \div 5.0$ eV, however, exceed our value 2.1 by a factor of ∼2. Another study by Müller[31] reported a comprehensive transport calculation using the TRANSIESTA package. The qualitative findings on the dependence of the conductance on contact geometry are consistent with our observations. However, a serious discrepancy prevails in the exponent, which was $\beta_N = 1.25$ in ref 31. In that study, the exponent together with the HOMO−LUMO gap, ∼17 eV, exceed considerably well-established experimental values ($\beta_N \approx 1.0$ and gap $\approx 8.5 \div 10.0$ eV[64]), which is hard to reconcile within a general expectation of LDA/GGA. An interesting attempt to go beyond the DFT approach for the conductance through alkanes was made by Fagas et al.[65] using a configuration interaction method. Unfortunately, the discrepancy between the obtained value, $\beta_N = 0.5$, and the experimental observation is even larger than the DFT-related uncertainty.

Discussion

Comparing Figures 5 and Figure 8A, we conclude that the *qualitative* agreement between experiment and theory is very good. Theory confirms the existence of three peak series in the experimental conductance histograms. The comparison of experimental observations and quantum chemical calculations suggests the following assignment: The M series of junction conductance data is attributed to an all-trans conformation of the alkyl chain and a double S−Au_1 contact geometry. The H series is assigned to an all-trans alkyl chain with the sulfur bound to two Au atoms on either side (S−Au_2 bridge−bridge geometry). The junction conductance between the two configurations differs by a factor of 4. Experimentally a factor of ∼5 was observed.

We expect that also mixed couplings (S−Au_2 on one side and S−Au_1 on the other) yielding a factor of roughly two in the conductance occur. An associated series is not necessarily easily distinguished experimentally, since its conductance peaks coincide with peak positions of the M and H series. We interpret the absense of clear indications for a mixed series in the experimental data as an indication, that the occurrence of mixed contact geometries is somewhat discouraged against the others by the experimental boundary conditions. Since only the all-trans conformation of the alkyl chains is involved for the M and H series of the junction conductance data, the decay of the conductance with the chain length is exponential with a theoretical decay constant $\beta_N = 0.83-0.88$ per CH_2 unit, which is very close to our experimental one $\beta_N = 0.94-0.96$. The latter value, ∼1, has been confirmed by a large number of experiments by now with single alkanedithiols as well as with alkanethiol monolayers.[16,22,30,39−45]

By contrast, the L series is much more complicated (Figure 4, refs 29,32). Our theoretical analysis suggests that gauge sites represent structural defects, which can lower the junction conductance up to a factor of 10 compared to all-trans alkyl chains. This trend is qualitatively not modified when assuming different contact geometries including short chains of gold adatoms. The experimentally observed ratio between M and L conductance data ranges between 34 for PD down to ∼2 for DD. In consequence, we assign these L conductance data to molecular junctions of various contact geometries with alkyl chains having at least one gauche defect. This manifests itself in a behavior of $G(n)$ which does not follow a simple exponential law. Additional support of our interpretation of the L series as an average over a certain ensemble of contact and gauge geometries might come from temperature-dependent transport measurements, ref 32. For the H and M series one may expect, that the leading T effect related to geometry is a modification of the relative probability to find an H vs M series. In fact, at sufficiently high T, an experimental current−distance curve (with relaxed molecules feeling no external forces) could show an average over different contact geometries, so that it no longer supports a clear plateau structure. By contrast, the L series should exhibit an additional average over gauche configurations at sufficiently large T. While in principle a great many configurations will be sampled, our calculations show that only very few—namely those with the largest conductance—dominate the transport average. As a consequence a roughly exponential dependence of the conductivity, $\sim\exp(-T_0/T)$, might be expected in a certain temperature range. Here, T_0 measures the typical energy cost for healing the wire from gauche defect(s). Indeed, this is the exponential dependency that has already been reported before in ref 32.

In addition, also the *quantitative* agreement for relative conductance values obtained from theory and experiment is reasonable, which is remarkable since simulations cover a broad range of conductance values. Theory appears to slightly underestimate the values of β_N, due to the reasons discussed above.

The discrepancy between theory and experiment in absolute values (contact conductance G_c) is a factor ∼5. Such deviations have been observed frequently before, and have been discussed in ref 50. Again, approximations in GGA most likely contribute to the error in the prefactor G_c.[66]

Finally, we comment on the occurrence of multiple steps in the measured conductance traces, which could be assigned to different junction geometries. We like to point out that we never observed an M step occurring after an L step or an H step

(60) (a) Lee, C.; Yang, W.; Parr, R. G. *Phys. Rev. B* **1988**, *37*, 785−789. (b) Becke, A. D. *J. Chem. Phys.* **1993**, *98*, 5648−5652. (c) Stephens, P. J.; Devlin, F. J.; Chabalowski, C. F.; Frisch, M. J. *J. Phys. Chem.* **1994**, *98*, 11623−11627.
(61) (a) Tao, J.; Perdew, J. P.; Staroverov, V. N.; Scuseria, G. E. *Phys. Rev. Lett.* **2003**, *91*, 146401. (b) Staroverov, V. N.; Scuseria, G. E.; Tao, J.; Perdew, J. P. *J. Chem. Phys.* **2003**, *119*, 12129−12137.
(62) Tomfohr, J. K.; Sankey, O. F. *Phys. Status Solidi B* **2002** *233*, 59−69; Tomfohr, J. K.; Sankey, O. F. *Phys. Rev. B* **2002**, *65*, 245105.
(63) Picaud, F.; Smogunov, A.; Dal Corso, A.; Tosatti, E. *J. Phys.: Condens. Mater. Phys.* **2003**, *15*, 3731−3740.
(64) (a) Fujimoto, H.; Mori, T.; Inokuchi, H.; Ueno, N.; Sugita, K.; Seki, K. *Chem. Phys. Lett.* **1987**, *141*, 485−488. (b) Less, K. J.; Wilson, E. G. *J. Phys. C: Solid State Phys.* **1973**, *6*, 3110−3120.
(65) Fagas, G.; Delaney, P.; Greer, J. C. *Phys. Rev. B* **2006**, *73*, 241314(R).
(66) (a) Burke, K.; Köentopp, M.; Evers, F. *Phys. Rev. B* **2006**, *73*, 121403. (b) Schmitteckert, P.; Evers, F. arXiv:0706.4253, preprint 2007.

occurring after an M step. The experimental current−distance traces only exhibit transitions from high- to low-conductance values. Transitions between H and M steps were observed frequently, while transitions from M steps to a single (or multiple) L step were observed very seldom. One trace, as an example, is plotted in Figure 3A. We suggest that the former (transitions between H and M steps) represent changes in the contact geometry as the junction is pulled apart. Changes in the molecular conformation appear to be rather improbable. Unfortunately, this hypothesis cannot be tested unambiguously for Au|alkanedithiol|Au junctions. Studies with metal electrodes and anchoring groups allowing only for one contact configuration because of geometrical or electronic reasons could help to resolve this open question in more detail.

Summary and Conclusions

We studied experimentally the conductance of single α,ω-alkanedithiols ($n = 5-10$) bound covalently to two gold electrodes in 1,3,5-trimethylbenzene (TMB) employing an STM-type break junction setup. The extracted conductance histograms revealed characteristic peaks corresponding unambiguously to *three sets* of distinct junction configurations, which were labeled L, M, and H. No preferential occurrence was observed under our experimental conditions. Within each sequence one could typically resolve up to three conductance peaks equally spaced at integer multiples of a fundamental conductance value.

The comparison with quantum chemistry ab initio simulations demonstrates that the multiple conductance values of Au|alkanedithiol|Au junctions could be attributed to different Au−sulfur coordination geometries and to different conformations of the alkyl chain. In particular, the medium conductance values M correspond to an all-trans conformation of the alkyl chain with one of the sulfur atoms coordinated in the atop position to a single Au atom. The high-conductance values H represent an all-trans alkyl chain in combination with both sulfurs coordinated to two Au atoms in bridge geometry. The sequence of low-conductance values L is attributed to nonequivalent isomers of alkanedithiols with gauche defects.

The experimental data and the ab initio quantum chemical simulations demonstrate that the M and H values fit to the exponential law $G(n) = G_c \exp(-\beta_N n)$. The experimental decay constants $\beta_N = 0.94 \div 0.96$ were found to be in good agreement with theoretical data. Nonexponential behavior was observed and explained for the L conductance junctions.

We emphasize that it was the combination of single-molecule conductance experiments with first-principle calculations that enabled us to develop a comprehensive and uniform understanding of microscopic details of charge transport in Au|alkanedithiol|Au junctions. In this way a proposal has been made for resolving contradictions between various literature reports.[16,22,23,25,29,30] We believe that results of our work have important consequences for the use of the conductance histogram technique in systems where several junctions with comparable conductance values can be realized, as is the case for molecules with isomeric structures. In such cases, peak series may occur which do not correspond to just a single species with single, double, triple, etc. junctions in parallel. Their interpretation may be feasible only with the assistance of elaborate ab initio simulations.

Acknowledgment. This work was supported by the HGF Project "Molecular Switches", the DFG, the Volkswagen Foundation, IFMIT and the Research Center Jülich. I.P acknowledges support of the German Academic Exchange Agency for a Ph.D. fellowship. F.E., A.A., and A.B. acknowledge support from the DFG "Center for Functional Nanostructures" situated at Karlsruhe University. We also acknowledge discussions with M. Mayor and A. Goerling.

Supporting Information Available: Additional material on the data analysis and the construction of histograms. This material is available free of charge via the Internet at http://pubs.acs.org.

JA0762386